DENSITY FUNCTIONAL THEORY APPROACH ON DYE DOPED KDP CRYSTALS FOR NON LINEAR OPTICAL APPLICATIONS

S.Rajeshkumar[1] & C.Tamil malar[2] & P.Kumaresan[3]
[1] P.G Department of physics, King Nandhivarman College of Arts and Science, Thellar-604406, Tamil Nadu, India
[1,2,3] P.G & Research Department of Physics, Thiru.A.Govindasamy Government Arts College, Tindivanam - 604 002 Tamil Nadu, India.

Received: December 09, 2018 Accepted: January 18, 2019

ABSTRACT: *Potassium Dihydrogen Phosphate (KDP) doped with dyes and it has been grown by slow solvent evaporation method at room temperature. The properties of the crystal have been improved by doping of organic impurities. In the present investigation, Pure and dye (Magneson I) doped KDP crystals are verified by Powder X-ray diffraction studies for phase analysis and structure determination. The presence of the functional groups has been identified by Fourier Transform Infrared spectrum (FTIR). The infrared absorption bands were identifying the molecular components and structures. The optical nature of the grown crystal is analyzed by using the UV-Visible spectrum. The UV-Visible spectrophotometer is used to determine the absorption or transmission of light by a sample.*

Key Words: *Crystal growth; KDP crystal; DFT Studies*

1. INTRODUCTION

Crystals are the root of modern technology. The modern technological development depends on the availability of suitable single crystals, whether it is for lasers, semiconductors, magnetic devices, optical devices, superconductors, telecommunication, etc. The needs of basic research and applications are developed over the years to meet the growth of single crystals [1-4]. The constituent molecules, atoms or ions in three dimensions are the regular periodic arrangement of the crystalline state. In nature the crystals are anisotropic. The properties of mechanical, electrical, magnetic and optical can differ according to the direction in which they were measured [5]. The crystals are used for devices because the charge carriers of electrons and holes which can move freely. The modern devices are very smaller and are made with higher yields. The improved yields come partly from device fabrication techniques and partly from improved materials. Most of the research works are going in manufacturing single crystals because the single crystals are the basic materials supporting the present advanced technologies and such research activities play an important role in manufacturing high-quality single crystals.

However, crystalline organic compounds represent a new class for technological applications. The organic materials have been of particular interest because the NLO responses in this broad class of materials are microscopic in origin, offering an opportunity to use theoretical modelling coupled with the synthetic flexibility to design and produce novel materials with low cost [6]. The relevance of organic materials in this context is because the delocalized electronic structure of π–conjugated organic compound offers a number of tantalizing opportunities in applications as NLO materials.

In the present investigation, Pure and dyes (Magneson I) doped KDP crystals are verified by Powder X-ray diffraction studies for phase analysis and structure determination. The presence of the functional groups has been identified by Fourier Transform Infrared spectrum (FTIR). The molecular components and structures are identifying by infrared absorption bands. By using the UV-Vis spectrum the optical nature of the grown crystal is analyzed. The UV-Visible spectrophotometer is used to determine the absorption or transmission of light by a sample.

2. EXPERIMENT

Crystal growth techniques are generally classified into three categories; they are growing from solution, growth from vapour and growth from the melt. All materials cannot be grown by all the above three methods because each growth techniques has numerous variations [7]. In my present work, the organic dye Magneson I were doped with KDP in 0.1% ratio and grow by slow evaporation technique at room temperature.

2.1 Solubility

It is most important that the study of solubility of the material in a suitable solvent before proceeding for the crystal growth. Solubility must be moderate and should have a positive temperature gradient in a selected solvent. The solubility of the pure and doped KDP in water was studied gravimetrically. The natural solvent water is mainly used as a solvent here. If the compound is not dissolved in water then the organic solvents such as acetone, methanol, ethanol etc are used.

2.3 Slow Evaporation Technique

In this popular technique, an excess of a given solute is founded by utilizing the difference between rates of evaporation of the solvent and the solute. A solution of the compound in a suitable solvent is prepared.

Moreover, in the cooling method, in which the total mass of the system remains constant, the solvent evaporation technique, the solution loses particles, which are infirmly bound to other components and therefore the volume of the solution decreases. In almost all cases, the vapour pressure of the solvent above the solution is higher than the vapour pressure of the solute and therefore the solvent evaporates more swiftly and the solution becomes supersaturated [8]. Usually, it is sufficient to allow the vapour formed above the solution to leave freely into the atmosphere. This is the primeval technique of crystal growth and technically, it is very simplistic.

The KDP salt was purified by repeated recrystallization using the method of dissolving in distilled water. Then the solution of KDP material was prepared in a more or less under saturation condition [9-12]. The solution was stirred well for four hours constantly using magnetic stirrer still the salt has been dissolved in water. Then the prepared solution was transferred into two clean Petri dishes and kept for crystallization at room temperature in a quiet place.

A supersaturated solution of pure KDP and 0.1% of Magneson I doped KDP at room temperature was obtained by constant stirring up to five hours and then filter into beakers. The satisfying quality seeds were pendulous in respective beakers using the nylon thread. Slow evaporation method was selected for the growth. After completion of growth run, the crystal was garner. The photograph of grown pure KDP and Magneson I doped KDP crystals are shown in **figure 1(a) and 1(b).**

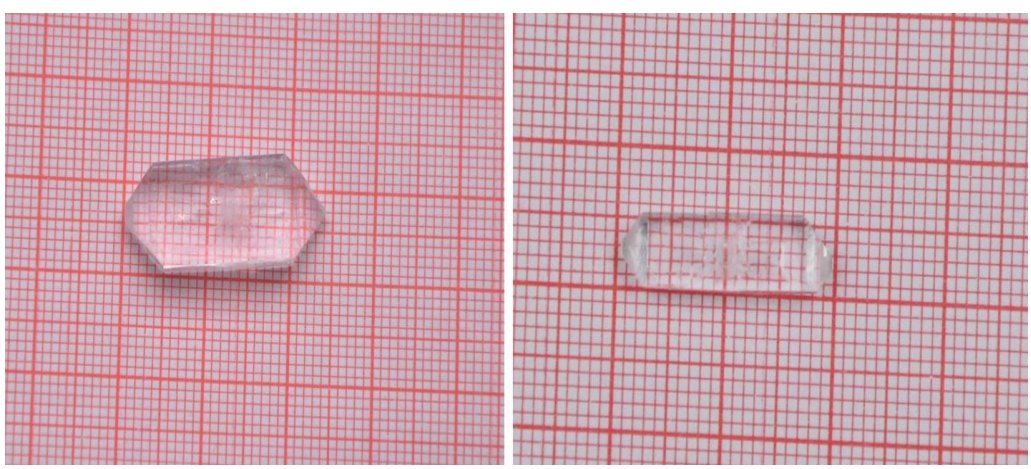

Figures 1(a) & 1(b).Pure KDP and Dye doped KDP Crystals

3. CHARACTERIZATION

3.1 Fourier Transform Infrared spectrum (FTIR)

The FTIR (Figure2) of all of them were recorded from solid phase samples on a Perkin Elmer-Spectrum 2 FTIR/ATR model spectrophotometer consists of globar and mercury vapour lamp as sources, with an interferometer chamber comprising of Mylar beam splitters and KBr followed by a sample chamber and detector. An entire region of 4000 – 450 cm^{-1} is covered by this instrument. The instrument has a typical resolution of 0.5 cm^{-1}. The Infrared spectrum is useful in identifying the functional groups like –OH, -CN, -CO, -CH, -NH2, etc. Also, quantitative estimation is occurring in certain cases for chemicals, pharmaceuticals, petroleum products, etc. From the below diagram graphical representation of the absorption spectrum of doped KDP samples are explained. In the specified region of 530 cm-1 mostly all the samples having the maximum absorption ranges.

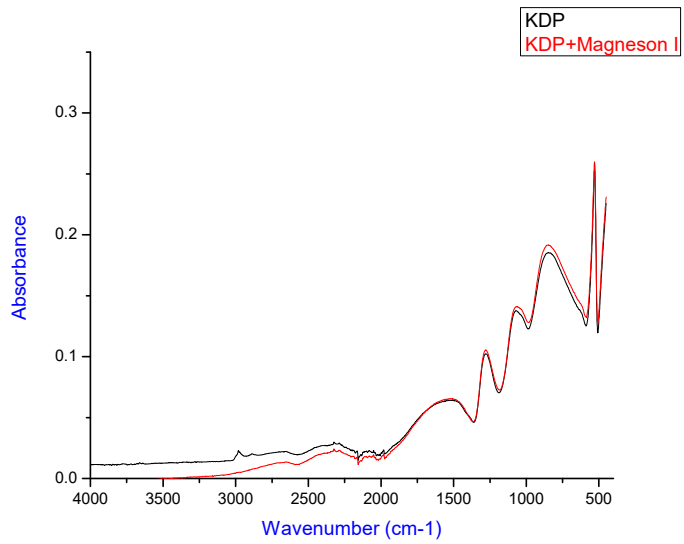

Figure 2. FTIR Spectra of Pure KDP and Magneson I doped KDP Crystal

3.2 UV – Visible Spectrum:

The UV – Visible spectroscopy of the pure KDP and doped KDP crystals was an analysis done by UV – visible spectrophotometer model of Lambda 35 UV Winlab spectrometer. The scanning range of this instrument is 190 – 1100nm and also it can be used to study single crystals and powder samples. By using a microprocessor this double beam instrument was controlled. The instrument has a bandwidth range 0.5 – 4 nm (variable). The spectrometer is well suited for samples both in solid and the dissolved form. The absorption spectrums for samples were measured over the wavelength range 200 nm to 900 nm. The graphs for absorption have been plotted in Figure 3. The pure and doped KDP crystals show a good absorption between 200 nm to 900 nm.

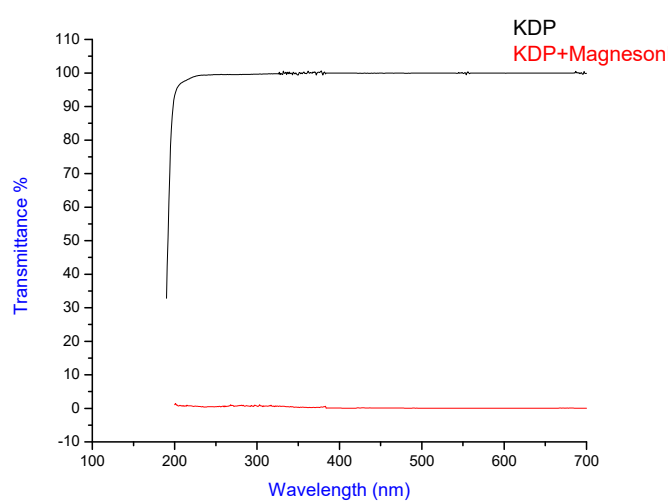

Figure 3. UV-Visible Spectra of Pure KDP and Magneson I doped KDP Crystal

3.3 Powder XRD Analysis:

Max von Laue, in 1912, discovered that crystalline material act as three-dimensional diffraction gratings for X-ray wavelengths related to the spacing of planes in a crystal lattice. For the study of crystal structures and atomic spacing, the X-ray diffraction is a common technique. X-ray diffraction is established on constructive interference of monochromatic X-rays and a crystalline sample [13]. These X-rays are produced by a cathode ray tube, filtered to generate monochromatic radiation, collimated to concentrate,

and directed toward the sample. The interaction of the incident rays with the sample produces constructive interference (and a diffracted ray) when the conditions satisfy Bragg's Law ($n\lambda=2d \sin\theta$). This law involves the wavelength of electromagnetic radiation to the diffraction angle and the lattice spacing in a crystalline sample. These diffracted X-rays are then detected, refined and counted. By scanning the sample through a range of 2θ angles, all possible diffraction directions of the lattice should be completed due to the random orientation of the powdered material [14-17]. The conversion of the diffraction peaks to d-spacing allows identification of the mineral because each mineral has a set of unique d-spacing. Typically, this is to implement by comparison of d-spacing with standard reference patterns.

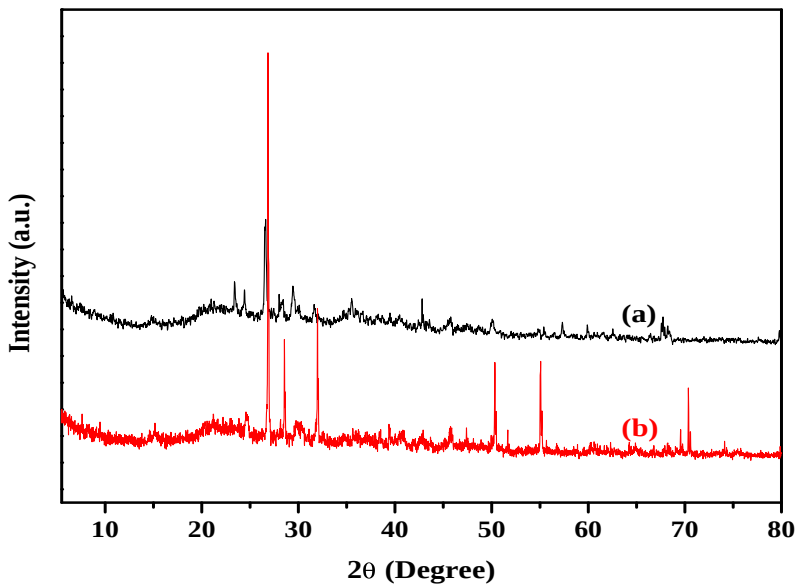

Figure 4. Powder XRD Spectra of Pure KDP and Magneson I doped KDP Crystal

All diffraction methods are based on a generation of X-rays in an X-ray tube. These X-rays are focused on the sample, and the diffracted rays are collected. The key component of all diffraction is the angle between the incident and diffracted rays. Powder and single crystal diffraction diverge in instrumentation beyond this. X-rays are produced in a cathode ray tube by heating a filament to generate electrons, accelerating the electrons toward a target by applying a voltage, and bombarding the target materials with electrons. When electrons have enough energy to dislodge inner shell electrons of the target material, characteristic X-ray spectra are produced.

This spectrum consists plenty of components, the most common being Kα and Kβ. Kα consists, in part, of $K\alpha_1$ and $K\beta_2$. $K\alpha_1$ has a slightly shorter wavelength 18 and twice the intensity as $K\beta_2$. The specific wavelengths are characteristic of the target material (Cu, Fe, Mo, Cr and Co). Filtering, by foils or crystal monochromaters, is needed to produce monochromatic X-rays need for diffraction. $K\alpha_1$ and $K\beta_2$ are sufficiently close in wavelength such that a weighted average of the two is used. Copper is the most common target material for single-crystal diffraction, with CuKα radiation = 1.54056 Å. These X-rays are collimated and focused into the sample. As the sample and detector are twisted, the intensity of the reflected X-rays is recorded. When the geometry of the incident X-rays appulsive the sample relieve the Bragg Equation, constructive interference occurs and a peak in intensity occurs. A detector records and processes this X-ray signal and changes the signal to a count rate which is then output to a device such as a computer monitor. For typical powder patterns, data is collected at 2θ from 10° to 70°, angles that all are present in the X-ray scan. The powder XRD analysis was analyzed by using XPERT-PRO analytical X-ray powder diffractometer.

3.4 HOMO and LUMO Analyses:

The highest occupied molecular orbital (HOMO) and lowest unoccupied molecular orbital (LUMO) are called the frontier molecule orbital's (FMOs) that has an important role in chemical reactions [18]. The HOMOs are donor groups filled by electrons, whereas the LUMOs are acceptor groups unfilled by electrons [19]. They use to interpret intramolecular charge transfers and molecular electronic transitions. The molecular electronic properties related to such as ionization potential, electron affinity, chemical reactivity, kinetic stability, polarizability, conjugation, chemical hardness and softness, chemical stability, aromaticity, chemical stability, electronegativity and electrophilicity index can be obtained using HOMO and LUMO energy values of the molecular systems[20-25].

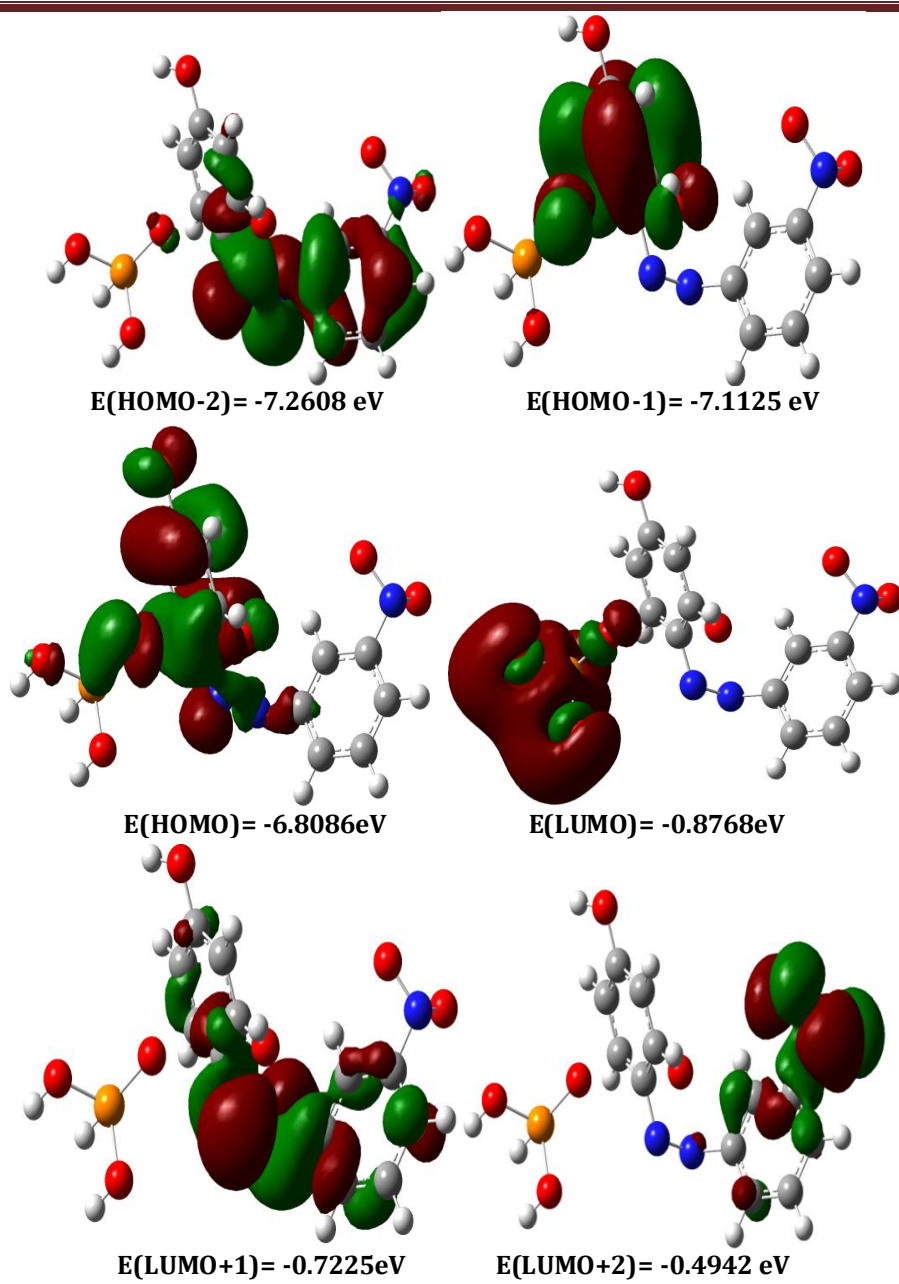

Figure 5. The simulated HOMOs and LUMOs plots and their energy values of Magneson doped with KDP.

The simulations of the HOMOs (H, H-1 and H-2) and LUMOs (L, L+1 and L+2) were computed using .chk file of the optimized molecular structure in chloroform with the B3LYP/6-311G (d,p) computational level. The simulated HOMOs and LUMOs plots and their energy values were given 372 in Figure 5. Additionally, the contributions to HOMOs and LUMOs of three molecular groups, which are Magneson doped with KDP were computed with chemissian software [26-28] and they were listed in Table 1. The HOMO, LUMO and HOMO-LUMO energy values were computed as -6.8086, -0.8768 and 5.9318 eV, respectively. As seen from Figure 6 and Table 1, both the HOMOs (H, H-1, H-2 and H-3) and the LUMOs (L, L+1 and L+2) were mainly localized over phenyl ring and KDP group. In general, the HOMOs were formed by p-bonding type molecular orbitals, whereas the LUMOs were formed by p-antibonding type molecular orbitals. The contributions to HOMO of Magneson doped with KDP and phenyl groups are 24%, 52% and 25%, while the contributions to LUMO of these groups are 10%, 30% and 61%, respectively. Similar comments can be made for other molecular orbital's. These contributions show that the abundance of the electron localizations on

KDP and phenyl ring of the title compound can be indicated the electronic transitions and charge transfers between these groups. Likewise, these molecular orbital formations of electron localizations on HOMOs and LUMOs are supported by π→π* and n→π* transitions in the experimental and simulated UV-Vis. spectra of the title compound.

Table 1. The contributions to HOMOs and LUMOs of the molecule groups in Magneson doped with KDP.

MOs	KDP	KDP doped
LUMO+2	17%	82%
LUMO+1	28%	55%
LUMO	10%	61%
HOMO	24%	25%
HOMO-1	8%	71%
HOMO-2	12%	82%

3.5 Molecular electronic potential maps

The electrostatic potential is indicant for molecule charge distribution in three-dimensions. Indeed this map enables people to diagnose and investigate the distribution of atoms charge in the different parts of the molecule. However, the prediction of behaviour and performance of the molecule in chemical reactions could be done by this map [29-34]. For calculating and displaying this map, initially the related structure has been optimized using density functional theory and in the following the electrostatic potential map has been calculated and recorded by Molekel program. From this map, it shows the modality of charge distribution for different parts of a molecule. The theoretical levels of B3LYP, for electrophilic and nucleophilic reactions are shown in Figs.6-8. Hydrogen atoms in this map have the minimum level of electrostatic potential and oxygen atoms have the maximum level of electrostatic potential. In addition, P atom is seen in green colour and is in the middle range of electrostatic potential level. In addition, nitrogen atoms related to the phenyl group is seen approximately yellow in the electrostatic potential map and approximately have more negative level than K atom.

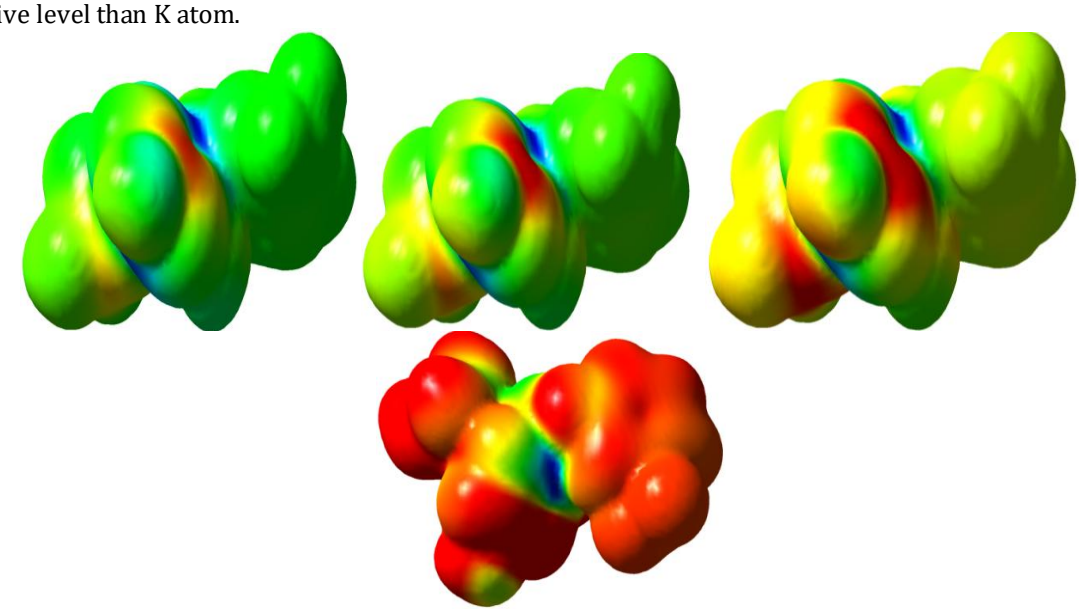

Figure 6. Different molecular electrostatic potential surface of Magneson doped with KDP

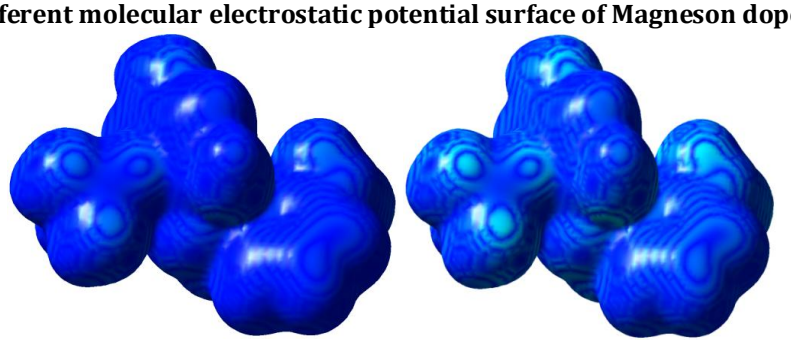

Figure 7.Different orientation of total electron density of Magneson doped with KDP

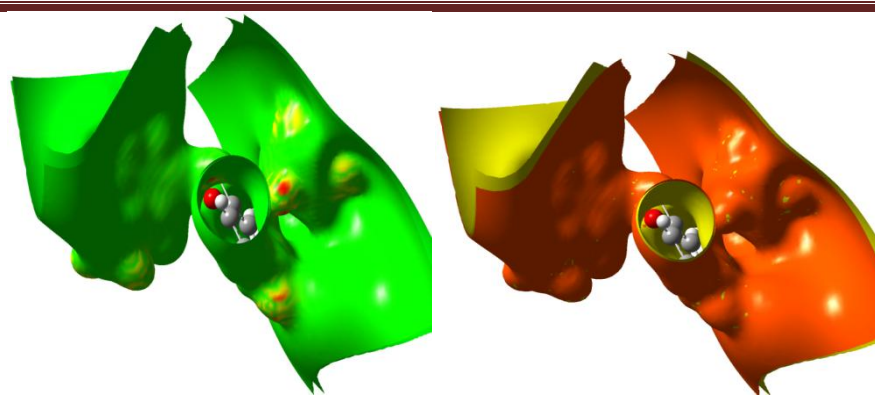

Figure 8.Different counter mapping surface of Magneson doped with KDP.

3.6 Atomic Charges

Mulliken and Natural atomic charges of Magneson doped with KDP were calculated with the DFT/B3LYP/6-311G (d, p) computation level using Mulliken and natural population analyses [35-37]. The computed atomic charges were summarized in Table 2. All hydrogen has positive charge values. They were computed at the intervals of 0.09788-0.13526 a.u. for Mulliken atomic charges and 0.19509-0.21418 a.u. for Natural atomic charges. Due to the electronegative property of oxygen atom, Mulliken and Natural atomic charges for O19 atom was obtained at -0.28929 a.u. and -0.54877 a.u., respectively.

Table 2.The computed Mulliken and Natural atomic charges of Magneson doped with KDP

Atoms	Mulliken	Natural
C1	-0.30516	-0.12624
C2	-0.11319	-0.38683
C3	-0.18386	-0.19558
C4	-0.15742	-0.38590
C5	-0.17830	-0.19156
C6	-0.16097	-0.38606
C7	-0.18067	-0.19557
C8	-0.11774	-0.37949
C9	-0.15146	-0.40353
C10	-0.15848	-0.38540
C11	0.18354	0.47619
C12	-0.27510	-0.15703
N13	-0.03731	-0.20032
N14	-0.08930	-0.19379
O15	-0.08825	-0.19015
O16	-0.09061	-0.19088
N17	0.00349	-0.18819
O18	0.13225	0.17239
O19	-0.28929	-0.54877
H20	0.21418	0.19917
H21	0.20525	0.11196
H22	0.19528	0.13029
H23	0.19528	0.11389
H24	0.20494	0.10853
H25	0.19539	0.10837
H26	0.19587	0.11429
H27	0.20563	0.10945
H28	0.20573	0.10922
H29	0.20291	0.11494
H30	0.20968	0.12682
P31	0.20515	0.12396

O32	0.19657	0.13526
O33	0.19509	0.12706
O34	0.21006	0.11121
O35	0.20309	0.10804
K36	0.20194	0.10570

434 The computed atomic charges for less electronegative sulfur atom were obtained as 0.13225 a.u. (Mulliken) and 0.17239 a.u. (Natural). The C11 carbon atom that is bonded to electronegative oxygen atom has a maximum positive charge with 0.118354 a.u. (Mulliken) and 0.47619 a.u. (Natural) values. The other carbon atoms bonded to positively charged hydrogen atoms have negative atomic charges at the intervals of (-0.03731)-(-0.30516) a.u. (Mulliken) and (-0.12624)-(-0.40353) a.u. (Natural).

3.7 Microhardness Measurements

The Magneson doped KDP crystals were subjected to Vicker's static indentation test at room temperature using Shimadzu (Model HMV 2T) hardness tester. Loads of different magnitudes ranging from 25g – 100g were applied for a duration of 5 seconds. Vickers hardness (VHN) is given by the relation

$$H_v = 1.854\ P / d^2 \ \text{(Kilogram / millimetre}^2\text{)}$$

Where P is the test load in kg, d is the mean diagonal length of indentation in mm and 1.854 is a constant of a geometrical factor for the diamond pyramid. Generally, the hardness of the material varies with the applied load. The applied indentation test load is balanced by the total specimen resistance composed of four components due to: (1) friction at the indenter/specimen facet interface (frictional component), (2) elastic deformation, (3) plastic deformation, and (4) specimen cracking.

The plot of Vicker's hardness (VHN) versus load (P) for the Magneson doped KDP crystal is shown in below figure 9. It is seen from the figure that the hardness value increases with an increase in the doping concentration. Also with the increase in indenter load, the hardness increases.

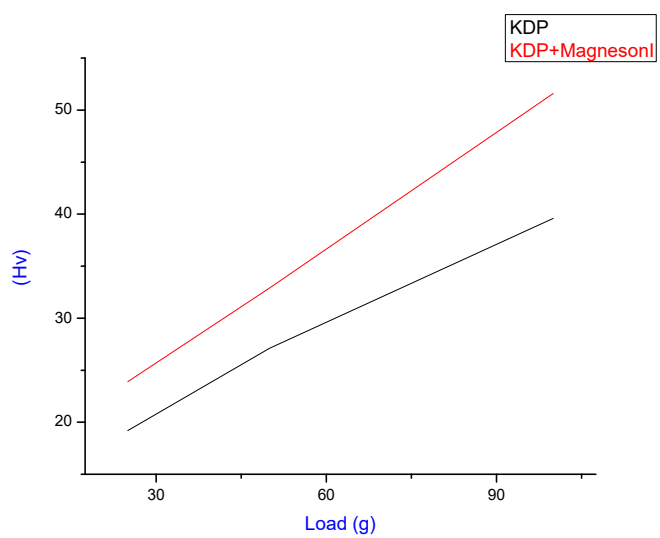

Figure 9. Microhardness of KDP doped with Magneson I

In the present work, microhardness of the pure and doped crystals is increased and reaches the saturation around 100 g of load and beyond which the materials undergo cracks. The mechanical properties of the doped crystal are increased compared with pure KDP crystals.

3.8 Dielectric studies

The dielectric study was carried out using LCRZ Meter unit in the frequency range of 50 Hz - 200 KHz. Figure 10-11 shows the plots of dielectric constant (ε_r) and dielectric loss ($\tan\delta$) versus frequency for pure and Magneson I doped KDP crystals. In the lower frequency region, the dielectric constant and dielectric loss have high values. The dielectric constant and dielectric loss both decrease as the frequency increases and at high-frequency region both remain almost constant, which is a normal dielectric behavior [38-42]. The relation of the dielectric constant (ε_r) was calculated by

$$\varepsilon_r = [\ Cd / A\varepsilon_o]$$

Where C is the capacitance value of the crystal, A is the area of the crystal under investigation, d is the thickness of the sample used and ε_o is the permittivity of free space.

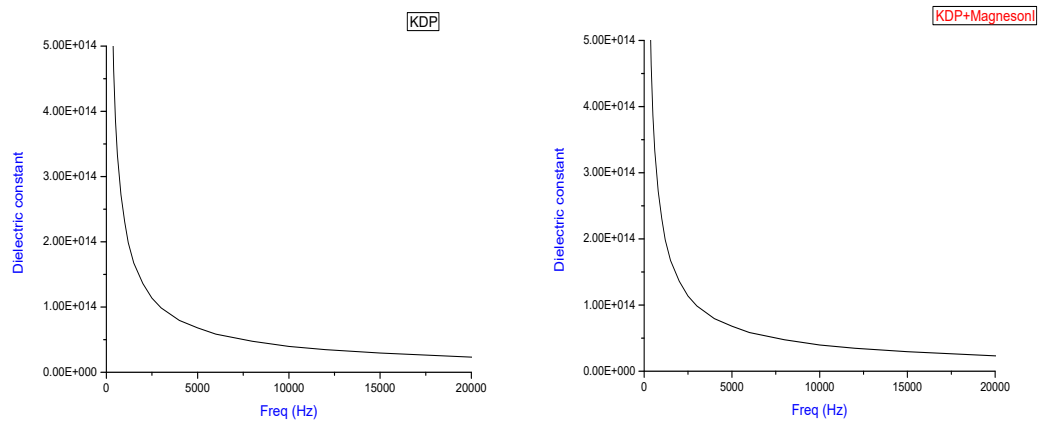

Figure 10. Dielectric constants for pure and doped KDP crystals

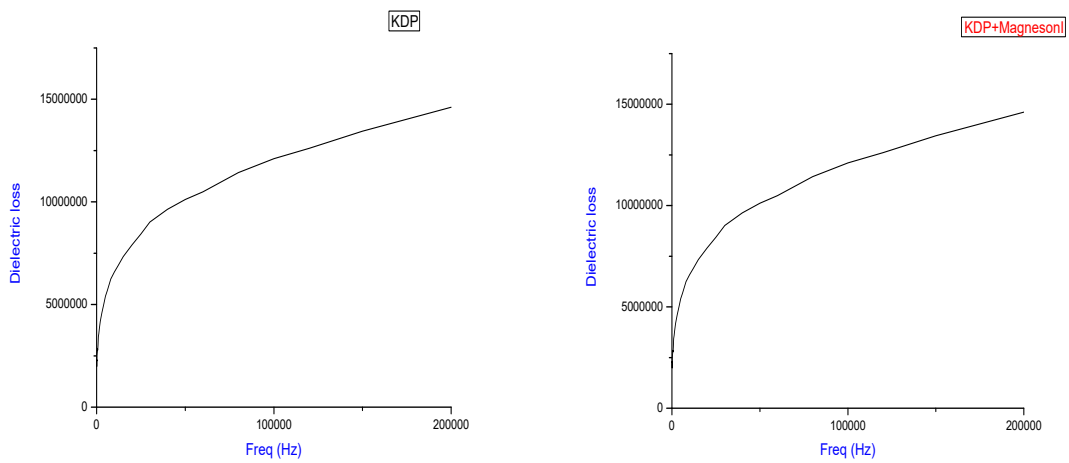

Figure 11.Dielectric losses for pure and doped KDP crystals

The loss tangent (tanδ) is a parameter of a dielectric material that quantifies its inherent dissipation of electromagnetic energy. The dielectric loss (ε") was given by

$$\varepsilon'' = \tan \delta \, \varepsilon_r$$

The dielectric constant and the dielectric loss of Magneson I doped KDP crystals are lower than the pure KDP crystals.

3.9 NLO Analysis:

The NLO reports of the samples are having high energy level comparing with pure KDP. The below table – 3 shows variations and energy level difference in the pure and doped samples. Dyes embedded in KDP crystal and dye doped crystal were also reported as useful non-linear optical media [43].

Table: 3 NLO Report

Sl. No.	Sample	Output Energy (milli joule)	Input Energy (joule)
1.	Pure KDP	8.94	0.70
2.	Magneson I doped KDP	11.81	0.70

The instruments specifications in Q switched High Energy of Nd:YAG Laser (Quanta ray Model LAB – 170 - 10) Model HG-4B- High efficiency, angle tuned and temperature stabilized Second harmonic and Third harmonic Generator Crystals. The Energy ranges are 850 mJ, 450 mJ & 220 mJ. The incident wavelength of the light is 1064 nm and the wavelength of the light emitted from the sample in this instrument is 532 nm. Instrument repetition rate was 10 Hz and the energy range is from 1.5 mJ to 3 J.

4. CONCLUSION

Good quality single crystals of pure and doped KDP were grown successfully by the slow evaporation technique. The Powder X-ray diffraction studies were carried out, and the lattice parameters are analyzed. Inductively coupled plasma studies show that the amount of dopant incorporated into the doped crystal is less than the concentration of the dopant in the corresponding solution. The pure and doped KDP crystals are transparent in the entire visible region and have minimum absorption. The MEP provides a visual method to understand the relative polarity of a molecule by mapping total density surface on electrostatic potential energy surface. Such surfaces depict the size, shape, charge density, and site of the molecules chemical reactivity. In this HOMO–LUMO energy gap and related molecular investigation, the more relevant electronic potential (IP), electron affinities (EA), chemical potential (μ) it is the negative of electronegativity (χ), hardness (η), softness (S) and the electrophilic index(ω) were calculated. In the Microhardness analysis, the pure and doped crystal is increased and reaches the saturation around 100 g of load and beyond which the materials undergo cracks. The mechanical properties of doped crystal are increased compared with pure KDP crystals. The dielectric constant and the dielectric loss of Magneson I doped KDP crystals are lower than the pure KDP crystals. The dielectric constant and dielectric loss have the high values in the lower frequency region. The dielectric constant and dielectric loss both decrease as the frequency increases and at high-frequency region both remain almost constant, which is a normal dielectric behaviour. NLO studies proved that the metal dopant has increased the efficiency of pure KDP. The presence of dopant has improved the Nonlinear optical (NLO) properties of the grown crystals and these crystals can be the promising material for nonlinear device fabrication.

REFERENCES

1. B. Latha, P. Kumaresan, S. Nithiyanantham, K. Sambathkumar J Molecular Structure 1152 (2018) 351-360
2. K. Sambathkumar, S. Nithiyanantham, J Mater Sci: Mater Electron (2017),28, 6529–6543.
3. Kuppusamy Sambathkumar Spectrochim. Acta A 147 (2015) 51-66.
4. D. Cecily Mary Glory, K. Sambathkumar, R. Madivanane , G. Velmurugan,R. Gayathri , S. Nithiyanantham, M. Venkatachalapathy, N. Rajkamal J of Molecular Structure 1163 (2018) 480-495.
5. A.Kumaresh, B.Arun kumar, Molecular & Bio Molecular Spec.111, 179(2013).
6. G.Ramasamy, S.P.Meenakshisundaram Ind. J. Pure Appl. Phys.122,pp 1121-1125(2013).
7. Pritula, A.Kosinova, Matrl.Res.Bulletin. 43 (2008) 2778-2789.
8. Z.Delci, D.Shyamala, Int.Nat J. Chem Res. Vol.4, No.2, 816-826 (2012).
9. T.Prasanyaa, M.Haris, Archives of Phy. Res, 2(4):60-66 (2011).
10. P.Jagdish, N.P.Rajesh, Jounl.of Opt Elec. Vol.13, No.8, (2011), 962-966.
11. B.Strukov, I.Shnaidshtein, Condensed Matter, Vol.10, No.1, (2007), 111-118.
12. A.Claude, V.Vaithinathan, Jounl.of Science. Vol.6, No.3, (2006), 635-638.
13. K.D.Parikh, D.J.Dave and M.J.Joshi, Modrn.Phy.Lett. B, Vol.23, 1589-1602,(2009).
14. P.Kumaresan, S.Moorthy Babu, Opt.Matter, Vol.30, 1361-1368 (2008).
15. P.Santhana Raghavan, P.Ramasamy, Recent Trends in Cry. Growth, Pinsa 68, (2002), p. 235.
16. J.Podder, S.Ramalingom, Crys.Res.Technol. 36 (2006) 549-556.
17. I.Pritula, A.Kosinova, Funct.Matrl. 14 No.3 (2007).
18. A.Bensouici, J.L.Plaza, Jounl.of Opt Elec. Vol.10, No.11, (2008), 3051-3053.
19. S.Javidi, M.Esmaeil Nia, Semi.con Phy Vol.11, No.4, 342-344 (2008).
20. P.Kumaresan, Jounl.Elec.Science & Tech, Vol.8, No.1 (2010).
21. L.M. Rouse, E.A.D. White, J. Cryst. Growth 34, 173 (1976).
22. S. Veintemillas Verdaguer, R. Rodriguez Clemente, J. Cryst. Growth 79, 198 (1986).
23. A.A. Zekic, M.M. Mitrovic, J. Cryst. Growth 258, 204 (2003).
24. Xun Sun, Xinguang Xu, Zhangshou Gao, Youjun Fu, Shenglai Wang, Hong Zeng, Yiping Li, J. Cryst. Growth 217, 404 (2000).
25. Chen Jianzhong, Lin Sukun, Yang Fengtu, Wang Jiahe, Lang Jianming, J. Cryst. Growth 179, 226 (1997).
26. S. Seif, K. Bhat, A.K. Batra, M.D. Aggarwal, R.B. Lal, Mater. Lett. 58, 991 (2004).
27. I. Owczarek, K. Sangwal, J. Cryst. Growth 102, 574, (1990).
28. O. Shimomura, J. Cryst. Growth 144, 253, (1994).
29. A. Yokotani, H. Koide, T. Sasaki, T. Yamanaka, C. Yamanaka, J. Cryst. Growth 67, 627, (1984).
30. Qing Zhang, F. Chen, and Nicholas Kioussis, S. G. Demos, H. B. Radousky, Physical Review B, **65**, 024108 (2001).
31. N.Y.Garces, K.T.Stevens, L.E.Halliburton, M.Yan, N.P.Zaitseva, J.J.DeYoreo, Journal of Crystal Growth **225,** 435 (2001).
32. A.Ryabov, N. Stelmakh, G. Pirogova, Y. Voronin, B. Zakharkin, 1991, Fiz.Tverd.Tela.**33**, 2660 – 2662 (in Russian)
33. Rashkovich L.N., KDP Family of Crystals. Hilger-Bristol, London, 1991.
34. Abe K., J. Phys. Soc. Jap., 1987, 56, 757.
35. Nakamura E., Ferroelectrics, 1992, 135, 237.

36. D. Rajan Babu, D. Jayaraman, R. Kumar, R. Jayavel, J. Cryst. Growth **245**, 121, (2003).
37. B. Latha, P. Kumaresan, S. Nithiyanantham , K. Sambathkumar Journal of Molecular Structure 1142 (2017) 255-260
38. M. Oftadeh, S. Naseh and M. Hamadanian, Computational and theoretical chemistry, Chemical Physics Letters, 966(2011), 20-25
39. K. Sambathkumar, S. Nithiyanantham, Synthesis, characterization and theoretical properties of coumarin NLO single crystal by DFT method J Mater Sci: Mater Electron 2017,28, 6529–6543
40. K.Sambathkumar, S.Jeyavijayan, M. Arivazhagan; Electronic structure investtigations of 4-aminophthal hydrazide by UV–visible, NMR spectral studies and HOMO–LUMO analysis by ab initio and DFT calculations Spectrochim. Acta A 147 (2015)51-66.
41. Keresztury G, Raman spectroscopy theory, in: JM Chalmers, P, Griffiths R (Eds.), Handbook of Vibrational Spectroscopy, Vol. 1, John Wiley & Sons Ltd., 2002, p. 71.
42. B. Latha, P. Kumaresan, S. Nithiyanantham ,K. Sambathkumar J Molecular Structure 1152 (2018) 351-360
43. K. Sambathkumar, S. Nithiyanantham, J Mater Sci: Mater Electron (2017), 28, 6529–6543.